Structure of the ATP-dependent oligomerization domain of N-ethylmaleimide sensitive factor complexed with ATP

Richard C. Yu[1], Phyllis I. Hanson[2], Reinhard Jahn[3] and Axel T. Brünger[1]

N-ethylmaleimide-sensitive factor (NSF) is a hexameric ATPase which primes and/or dissociates SNARE complexes involved in intracellular fusion events. Each NSF protomer contains three domains: an N-terminal domain required for SNARE binding and two ATPase domains, termed D1 and D2, with D2 being required for oligomerization. We have determined the 1.9 Å crystal structure of the D2 domain of NSF complexed with ATP using multi-wavelength anomalous dispersion phasing. D2 consists of a nucleotide binding subdomain with a Rossmann fold and a C-terminal subdomain, which is structurally unique among nucleotide binding proteins. There are interactions between the ATP moiety and both the neighboring D2 protomer and the C-terminal subdomain that may be important for ATP-dependent oligomerization. Of particular importance are three well-ordered and conserved lysine residues that form ionic interactions with the β- and γ-phosphates, one of which likely contributes to the low hydrolytic activity of D2.

N-ethylmaleimide-sensitive factor (NSF) is an evolutionarily conserved ATPase that is required for intracellular trafficking and fusion events. Based on *in vitro* assays for vesicular transport between Golgi-membranes, NSF was originally thought to be directly involved in membrane fusion[1,2]. More recently, however, NSF's action has been implicated in priming membranes for fusion — that is, acting before membrane docking and fusion occurs[3–5]. Before NSF can act, soluble co-factors, termed SNAPs (soluble NSF attachment proteins) must bind to certain membrane protein targets which then mediate the binding of NSF. These targets include a group of membrane proteins, termed SNAP receptors (SNAREs)[6], which are essential components of membrane fusion complexes. Many isoforms of SNAREs localize to different subcellular membranes, supporting the view that SNAREs are involved in most, if not all, eukaryotic fusion events. Complementary sets of SNAREs are present on the membranes destined to fuse and spontaneously assemble into tight complexes. This assembly reaction probably results in membrane docking and may drive the fusion reaction itself[7]. NSF disassembles these complexes after ATP hydrolysis, resetting the SNARE proteins for another round of membrane docking and fusion.

High-resolution structural studies are needed in order to elucidate the molecular mechanism by which NSF dissociates the SNARE complex. This paper represents a first step towards this goal. NSF is a hexamer[7] consisting of six identical subunits with a distinct domain structure, resembling proteins from the AAA (ATPases associated with cellular activities) family[8,9]. AAA proteins such as p97, VCP, and Hsp104 are involved in cellular trafficking and protein disassembly, and are characterized by containing one or two 230 amino acid ATP binding cassettes. Each NSF protomer (83,000 M_r) contains an N-terminal domain responsible for the interaction with α-SNAP and the SNAREs, a low-affinity ATP-binding domain, termed D1, whose hydrolytic activity is associated with NSF-driven SNARE complex disassembly, and a C-terminal high-affinity ATP-binding domain, termed D2[10]. Although the D2 domain is able to hydrolyze ATP at a very low rate[11], there is no evidence for a requirement of this hydrolytic activity in SNARE complex disruption. Rather, the D2 domain, highly conserved among the NSF family (Fig. 1), appears to be responsible for the formation of the NSF hexamer[12–14]. NSF is active only as a hexamer, and likely utilizes all protomers during disassembly[13].

Nucleotide depletion by apyrase incubation leads to a dissociation of NSF into monomers, as suggested by electron micrographs (P.I. Hanson, unpublished results). Additionally, electron micrographs show major conformational changes between the ADP- and ATP-bound forms of the NSF hexamer, most likely due to the movement of the N-terminal domain[7]. The buildup of conformational 'tension' in the hexamer upon D1 ATP binding may be utilized in the disruption of the SNARE complex. Thus, SNARE complex disruption is probably mediated by the α-SNAP-binding N-terminal domain in concert with the ATP-hydrolyzing D1-domain, while the D2-domain keeps the oligomer intact. It cannot be ruled out, however, that some ATP hydrolysis by the D2 domain occurs during complex disruption.

Here we report the crystal structure of the bacterially expressed D2-domain of NSF complexed with ATP at a resolution of 1.9 Å. The structure confirms the oligomeric state of the molecule and reveals a six-fold molecular symmetry axis. The structure provides a likely explanation for the slow hydrolytic rate, and it suggests how ATP binding promotes oligomerization of the NSF D2 domains.

Structure determination

Native and selenomethionine (SeMet) versions of recombinant histidine-tagged NSF-D2, containing residues 486–744 of the full-length Chinese hamster ovary NSF sequence[15], were overexpressed in *E. coli*, purified to homogeneity after tag

[1]The Howard Hughes Medical Institute and Department of Molecular Biophysics and Biochemistry,Yale University, New Haven, Connecticut 06520, USA. [2]Department of Cell Biology and Physiology,Washington University School of Medicine, St. Louis, Missouri 63110, USA. [3]Department of Neurobiology, Max-Planck-Institute for Biophysical Chemistry, D-37077 Göttingen, Germany.

Correspondence should be addressed to A.T.B. *email: brunger@laplace.csb.yale.edu*

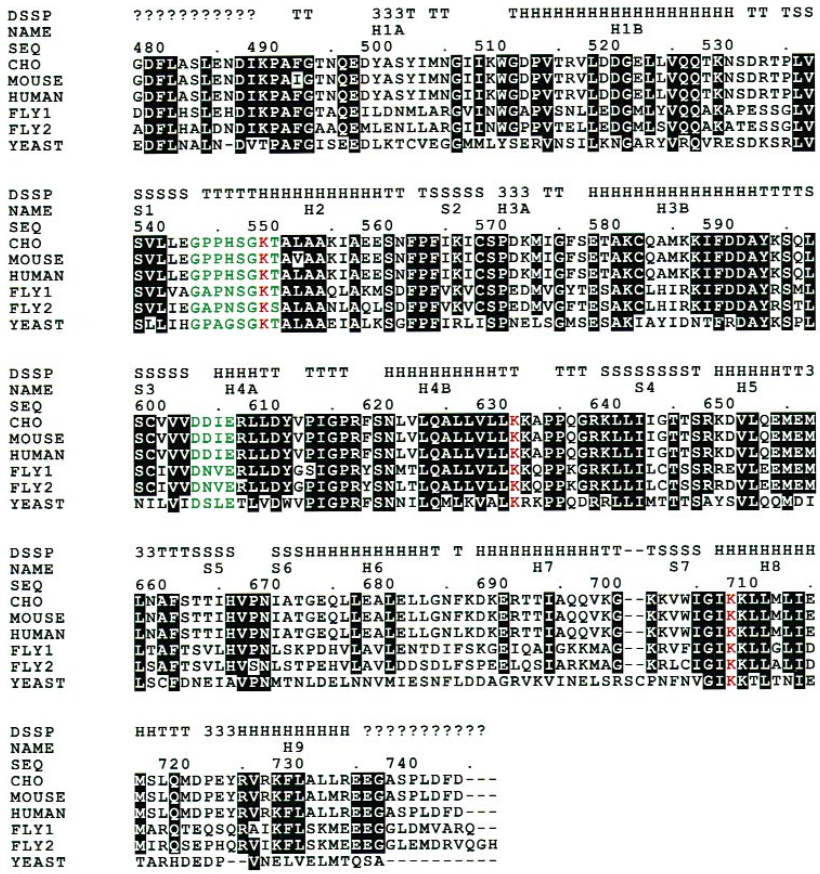

Fig. 1 Sequence alignment of NSF homologs from Chinese Hamster Ovary (SWISSPROT-P18708), mouse (P46460), human (P46459), fly isoform 1 (P46461), fly isoform 2 (P54351) and yeast (P18759). Highlighted in green are the Walker A and Walker B nucleotide binding consensus sequences, and in red are conserved ATP-interacting residues Lys 549, Lys 631, and Lys 708. The first row of each block is a DSSP[39] determined secondary structure assignment ("?" for disordered residues, "T" for turn, "3" for 3_{10}-helix, "H" for α-helix,and "S" for β-strand). The second row contains names for helix or sheet secondary structure elements. Alignment made using CLUSTALW[40] and BOXSHADE[41].

cleavage, and crystallized by hanging drop vapor diffusion. The structure of NSF-D2 was solved using SeMet multi-wavelength anomalous dispersion (MAD) phasing[16] to 2.4 Å and subsequent phase-extension was carried out to 1.9 Å using native diffraction data. All selenium sites except for a disordered N-terminal methionine were found using a Patterson search method (R.W. Grosse-Kunstleve and A.T.B., unpublished). The excellent quality of the experimental 2.4 Å map (Fig. 2*a*) and knowledge of the selenium positions allowed for nearly complete initial main chain tracing and side chain positioning, and served as a validation tool in difficult regions during model rebuilding. The experimental map also clearly revealed most side chain positions involved in interactions with the nucleotide that may be important for ATP-dependent oligomerization.

Overall topology

Recent solution studies showed NSF's oligomeric state to be hexameric[17]. Low-resolution electron micrographs have confirmed this hexameric morphology in wild-type NSF and in isolated D2 domain preparations[7], and similar studies of the p97 homologue also show a clear six-fold symmetric arrangement[18]. The high-resolution crystal structure of D2 is hexameric, with the crystallographic six-fold symmetry axis coincident with the molecular one. It also reveals extensive interactions between the triangle-shaped protomers (Fig. 3), which bury over 1,100 Å^2 of surface area per interface per protomer.

An NSF protomer consists of two distinct subdomains (Fig. 4*a*,*b*). The N-terminal subdomain exhibits a common nucleotide binding motif[19] consisting of a parallel β-sheet surrounded by α-helices. A DALI[20] structural similarity search indicated homology between this subdomain and other Rossmann-fold containing proteins, with the closest match being the δ'-subunit of *E. coli* DNA polymerase III[21] . In loops between β-strand S1 and α-helix H2 and between β-strand S3 and α-helix H4a, there are nucleotide consensus binding and catalysis sequences GXXXXGK[S/T] and YYXY respectively (where X are hydrophobic and Y are acidic residues), also known as Walker A and Walker B consensus sequences[22]. The C-terminal subdomain, which contacts one of the two adjacent protomers (Fig. 3*b*), may be a crucial link between nucleotide binding and hexamerization.

Pore

The hexamer forms a pore that tapers from ~30 Å, at the side of the D2 domain connected to the D1 domain in full-length NSF (top in Fig. 4*c*), to ~18 Å at the other side. The pore is predominantly negatively charged with a positively charged arginine residue (Arg 617) in the middle (Fig. 4*c*). This arginine side chain, following a tight turn containing a glycine (Gly 615) followed by a *cis*-proline (Pro 616) between α-helices H4a and H4b (Fig.5*a*), forms a hydrogen bond with the backbone oxygen of Phe 618 of a neighboring protomer, possibly contributing to the stability of the hexamer.

Interactions between NSF, α-SNAP, and SNARE receptors have been shown to be important for membrane fusion. A current model suggests that NSF and α-SNAP bind to a SNARE complex and induce conformational changes that dissociate the complex and prime the membranes for fusion[7,23]. NSF and α-SNAP, preincubated with ATP-γ-S, a non-hydrolyzable ATP analog, are seen in electron micrographs bound at one end of a SNARE complex. The crystal structure of the core synaptic fusion complex, a minimal version of the SNARE receptor complex, was recently solved to 2.4 Å resolution (R.B. Sutton, D.Fasshauer, R.J., and A.T.B., submitted). This complex has a rod-like shape with a length of approximately 115 Å and a diameter that varies between 20 Å and 25 Å; it also has numerous negatively charged surface residues. Direct binding of the core fusion complex inside the D2 pore is thus unlikely unless

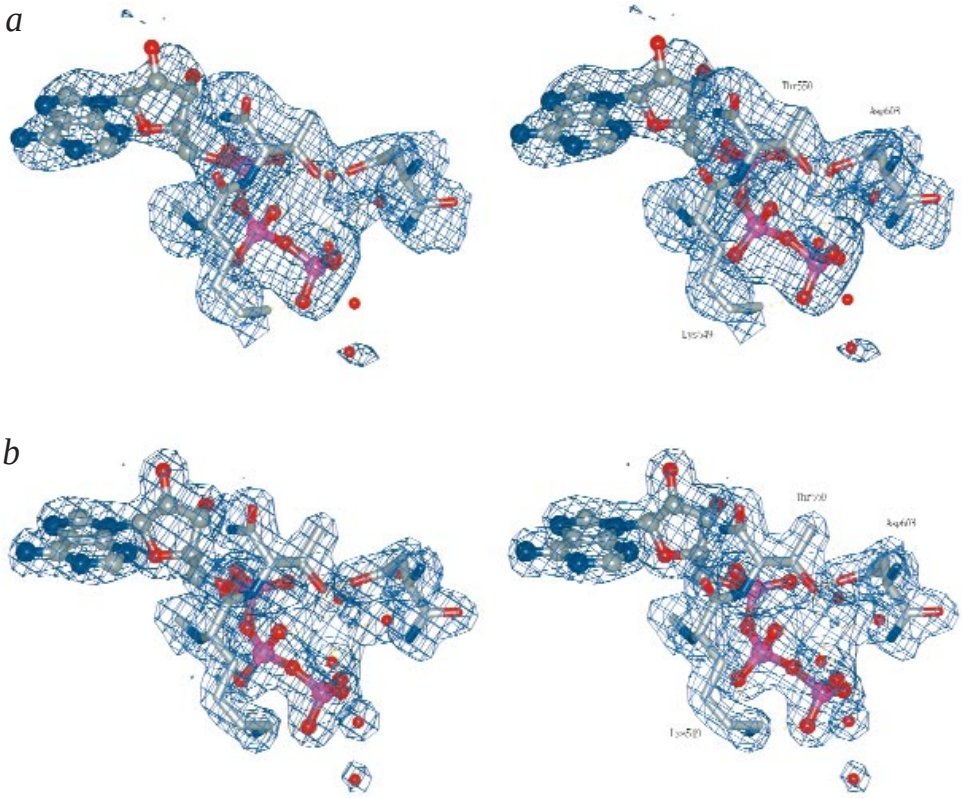

Fig. 2 Electron density maps around the ATP binding site, contoured at 1.25 σ. Magnesium ion, in white, is coordinated by Thr 550, three water molecules (one of which is coordinated by Asp 603), and β- and γ-phosphate oxygens. Prepared using gl-render, Bobscript[42], and rendered using POV-ray[43]. ***a***, Stereoview of experimental electron density map using MAD phases. ***b***, Stereoview of phase-combined $2F_o$-F_c σ_A-weighted electron density maps using MAD and model phases of the refined model.

NSF and the fusion complex undergoes significant conformational changes in order to fit into the pore. Other factors such as α-SNAP or divalent cations would have to compensate for the charge distribution.

ATP Binding Site

The ATP nucleotide is bound at the junction of the N-terminal and C-terminal subdomains of one protomer and the N-terminal subdomain of a neighboring protomer (Figs 3*a*,*b* and 5*b*). The purine base binding pocket is primarily hydrophobic, with the exception of a hydrogen bond between the backbone oxygen of Ile 508 and the N6 nitrogen of the ATP (providing a means to distinguish between ATP and GTP), and a water-mediated hydrogen bond between Trp 510 and the backbone oxygen of Ser 507. The ATP is in a *syn* conformation, in contrast to the nucleotide conformation in the 2.4 Å GroEL chaperonin crystal structure complexed with ATP-γ-S[24]. The ribose has a major C2'-endo, minor C3'-exo sugar pucker, which is favored in *syn*-conformation nucleotides.

The protein–triphosphate tail interactions are similar to what is found in other nucleotide binding proteins. All interacting α-helices are oriented with their N-termini towards the negatively charged phosphates (Fig. 4*a*,*b*). A conserved Walker A sequence, of the form GXXXGK[T/S], is located between β-strand 1 and α-helix 2, with the conserved Lys 549 electrostatically interacting with β- and γ-phosphates (Figs 1, 2*a*,*b*, 5*b*). This lysine has been implicated in nucleotide binding in other ATP binding proteins[25], and mutations of this lysine in full-length NSF significantly reduces *in vitro* intra-Golgi transport activity[12,13]. A catalytic magnesium ion is coordinated by three water molecules (one of which hydrogen bonds with Asp 603), Thr 550, and the β- and γ-phosphate oxygens. A small pocket of hydration sites is close to the γ-phosphate, with three water molecules within 4 Å of the γ-phosphorus.

Another conserved lysine from one of the neighboring protomers, Lys 631 (Figs 1, 5*b*,*c*), may affect the ATPase activity of NSF-D2. Metal ions interacting with the β- and γ-phosphates are generally thought to stabilize the transition state and anionic products of ATP hydrolysis. Indeed, the magnesium ion is in the expected position for such an electrostatic stabilization. This charge distribution may be perturbed by Lys 631, enough to reduce the catalytic effect of the coordinated Mg^{2+} on hydrolysis. Lys 631 may also hinder nucleophilic water molecules from attacking the γ-phosphate, both by occupying space near the target and by discouraging deprotonation of the attacking water molecule.

ATP-dependent hexamerization

Contact areas between NSF-D2 protomers contain hydrogen bonds and hydrophobic patches between the neighboring N-terminal Rossmann-fold subdomains, formed by the aliphatic side chain region of Lys 586, Leu 609, Phe 618, Leu 623, and Val 628 on one protomer and Ile 574, Val 612, and Ile 614 on the other (Fig. 6*a*,*c*). Additional hexamer-stabilizing interactions include salt bridges formed between Arg 648, on the loop between β-strand S4 and α-helix H5, and Glu 656, on α-helix H5 on a neighboring subunit, in a region close to the ATP binding site.

There are two ATP–protein interactions that may explain ATP stabilization of the hexamer. The Lys 631 γ-phosphate bond mentioned above is an obvious ATP-dependent intersubunit interaction. A third conserved lysine, Lys 708, in the

C-terminal subdomain directly contacts the γ-phosphate of the bound ATP (Fig. 5*b*,*c*). This ionic interaction may help position the C-terminal subdomain, in addition to a hydrophobic contact region formed between the N-terminal and C-terminal subdomains, consisting of side chains from Ile 508 and Trp 510 from the former, and Ile 670, Leu 682 and Leu 683 from the latter (Fig.6*a*,*b*).

These lysine–ATP interactions may also contribute to the low dissociation constant of ATP. After purification, the protein, at a concentration of 4 mg ml^{-1}, was dialyzed for 24 h at 4 °C against buffer containing 20 mM ADP as the sole nucleotide, well above the 140 μM dissociation constant for ADP, determined at room temperature[26]. The experimental electron density map clearly shows triphosphate, not diphosphate, connectivity for the nucleotide (Fig. 2*a*). B-factors for the γ-phosphate atoms are similar to those for α and β-phosphate atoms, so the crystal probably does not contain a mixture of ATP- and ADP-bound NSF-D2 molecules. These observations indicate that even under conditions where ATP binding is thermodynamically unfavorable, ATP is kinetically trapped.

We propose the following model for hexamer destabilization after ATP hydrolysis or depletion. After the loss of the Lys 708 ATP β/γ-phosphate interaction, the C-terminal subdomain position would be maintained primarily by the two hydrophobic patches mentioned above. It would then be more likely to move, perhaps by sliding along the non-specific hydrophobic interfaces or, if the interfaces are disrupted, by swinging about the linker region consisting of residues between β-strands S5 and S6.

In addition to losing the interaction between Lys 631 from the neighboring protomer to the ATP this large, putative conformational change would shift the oligomerization equilibrium towards the monomeric state. Electrostatic repulsion by the lysines in the nucleotide binding pocket after ADP dissociation would contribute to this destabilization. While NSF-D2 alone has low ATPase activity, perhaps conformational changes in the full length hexamer or binding of additional co-factors increase the hydrolysis rate and promote hexamer dissociation.

Conclusions

The D2 domain of NSF is known to be essential for hexamerization. The crystal structure suggests how ATP binding may stabilize the hexamer. Three well-ordered lysines, conserved

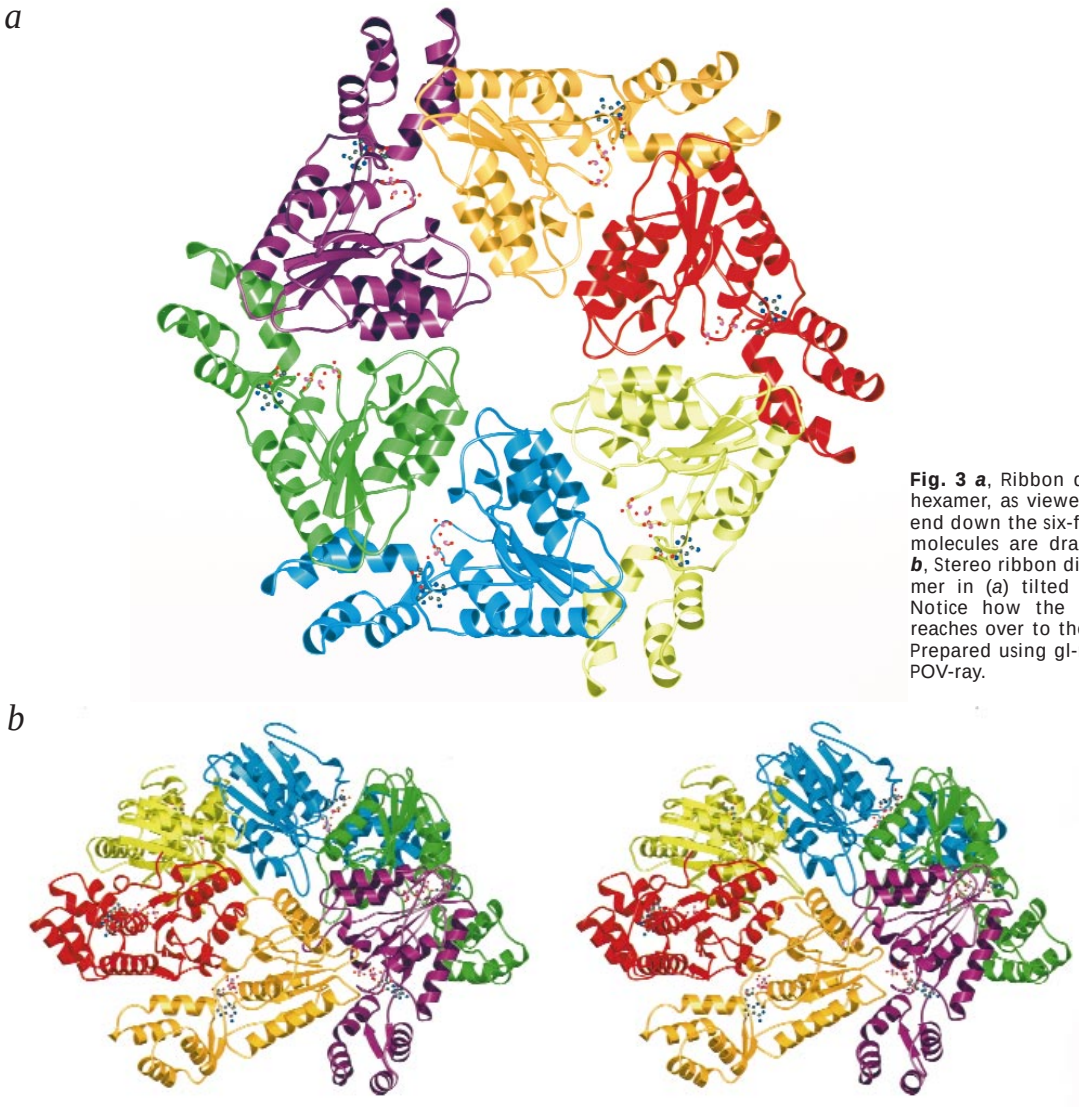

Fig. 3 ***a***, Ribbon diagram of the NSF-D2 hexamer, as viewed from the N-terminal end down the six-fold symmetry axis. ATP molecules are drawn as balls-and-sticks. ***b***, Stereo ribbon diagram of NSF-D2 hexamer in (*a*) tilted -50° along the Y-axis. Notice how the C-terminal subdomain reaches over to the neighboring subunit. Prepared using gl-render, Molscript[44] and POV-ray.

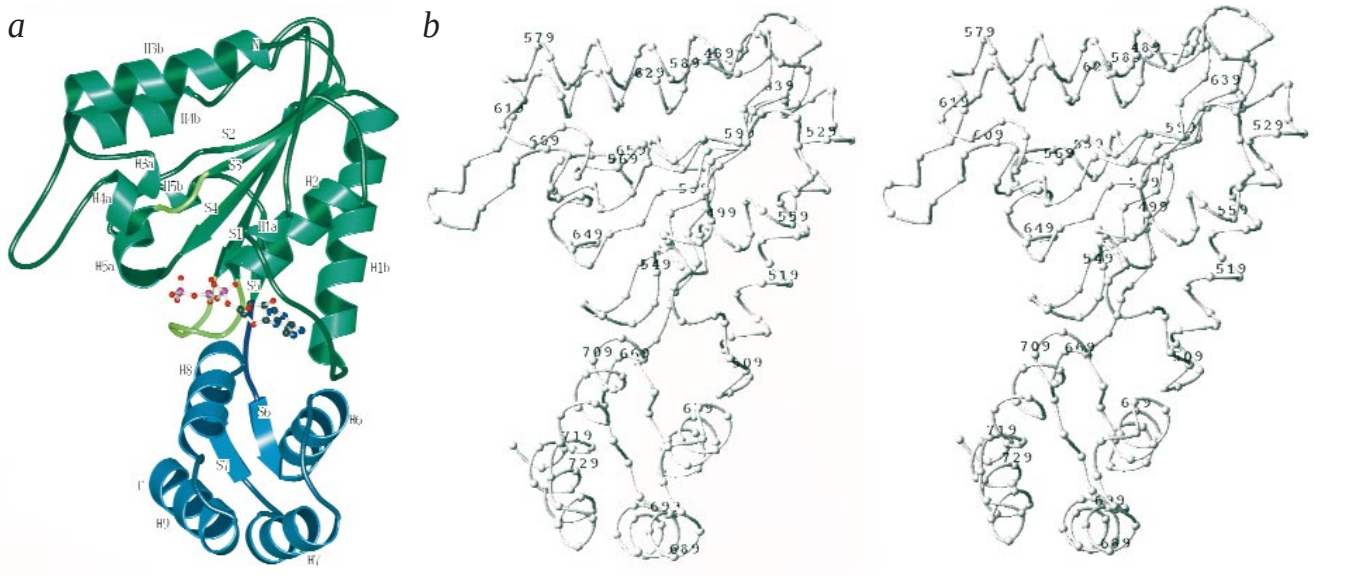

Fig. 4 ***a***, Ribbon diagram of theNSF-D2 protomer consisting of two subdomains, an upper N-terminal subdomain in green and a lower C-terminal subdomain in blue-green. The N-terminal region consists of a Rossmann fold, a series of secondary structure elements that form a central parallel β-sheet surrounded by α-helices, in the order as found in the primary sequence: 3_{10}-helix 1a (H1a), α-helix 1b (H2b), β-strand 1 (S1), H2, S2, 310 H3a, H3b, S3, H4a, H4b, S4, H5a, H5b, and S5. The C-terminal subdomain consists of a four-helix bundle and a small two-strand antiparallel sheet: S6, H6, H7, S7, H8, and H9, ordered in primary sequence space. The Walker A (between S1 and H2) and B (between S3 and H4a) ATP binding consensus sequence regions are shown in light green. The N-terminus is marked 'N'. Prepared using gl-render, Molscript and POV-ray. ***b***, Cα stereoview of the D2 protomer, with every tenth residue indicated. Prepared using MOLMOL[45]. ***c***, GRASP[46]-calculated surface electrostatic potential along the pore. Negative charges (red) dominate the pore, particularly at the 'top' (which would be connected to the D1 domain in full-length NSF), with the exception of a positive charge (blue) associated with Arg 617. Hydrogens were positioned using CNS, and the surface potential calculated using the OPLS[47] charge parameter set distributed with GRASP. Surface potential color ranges from -10 kT/*e* (red) to 10 kT/*e* (blue).

in NSF homologs, form ionic interactions with the nucleotide triphosphate tail. The first is from the N-terminal subdomain in a conserved Walker A motif. The second is from the neighboring protomer which interacts with the γ-phosphate, and may interfere with the hydrolytic activity of D2 by destabilizing the transition state of the hydrolysis reaction or by hindering nucleophilic water molecules. It may also contribute an ATP-dependent interaction between protomers. The third originates from the C-terminal subdomain and also interacts with the γ-phosphate. Upon ATP hydrolysis, the weakening of this ionic interaction may allow the C-terminal subdomain to more easily dissociate from the neighboring subunit, destabilizing the hexamer.

While the role of D2 in NSF-mediated SNARE disassembly is not known, the crystal structure reveals that the D2 hexamer pore could not accommodate the synaptic fusion complex, whose crystal structure was recently determined (R.B. Sutton, D.Fasshauer, R.J., and A.T.B., submitted), without significant structural changes.

Note added in proof: The structure of AMP-PNP bound NSF-D2 has been independently solved by another group[38].

Methods

Expression and purification. A TEV-protease cleavable hexahistidine-tagged NSF-D2 fusion protein was obtained as follows. PCR was performed using primers 5'-GGA ATT CCA TAT GGG AGA CTT CCT GGC TTC TTT GG-3' (sense strand) and 5'-GAA TTC CTG ATC ACT CGA GAT CAA AGT CCA GGG GGC TAG CG-3' (antisense) and the pQE9-CHO NSF plasmid (obtained from J. Rothman) as a template. The resulting PCR product was subcloned into pProEX-1 (Life Technologies, Inc.) using the NdeI and XhoI restriction sites. The NcoI/EcoRI restriction fragment containing the hexahistidine tag, TEV protease site, and NSF-D2 was cloned into pET-28b (Novagen). The DNA sequence was verified by dideoxynucleotide sequencing. The protein was overexpressed in BL21(DE3) *E. coli* cells (Novagen). Cells were grown in a BioFlo 3000 10 liter fermenter (New Brunswick Scientific) at 30 °C in ECPM1 media[27] with 50 mg ml^{-1} kanamycin and induced with 0.8 mM isopropyl-1-thio-galactopyranoside (IPTG) at an optical density of A_{600nm} = 25. After 4 h, the cells were harvested by centrifugation and flash-frozen in liquid nitrogen. 50 g cells were thawed and homogenized in 200 ml buffer A (20 mM HEPES 7.0, 500 mM NaCl, 0.1 mM ATP pH 7.0,1 mM $MgCl_2$, 1 mM β-mercaptoethanol) supplemented with 1 mg ml^{-1} lysozyme, 0.1% Triton X-100, and 10 mg ml^{-1} DNaseI. After 30 min of gentle stirring at 4 °C, the lysate was centrifuged for 30 min at 40,000 g. The supernatant was gravity loaded onto a column packed with 10 ml of buffer A equilibrated Ni-NTA resin (Qiagen). The column was washed with 20 ml buffer A with 10 mM imidazole (pH 7.0), and the protein eluted with a linear gradient from 10–300 mM imidazole (pH 7.0).

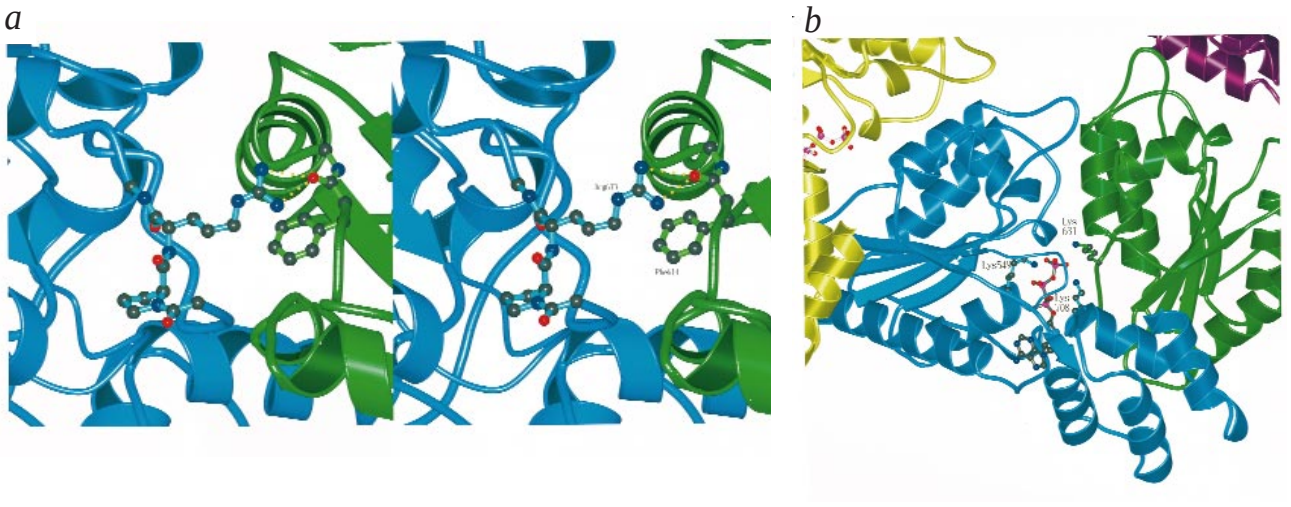

Fig. 5 ***a***, Molscript and POV-ray rendering of the hydrogen bonds between Arg 617 from one protomer (blue) and the Phe 618 backbone oxygen from the neighboring protomer (green) in the pore of the D2 domain. ***b***, Ribbon diagram illustrating positions of three conserved lysines around the triphosphate tail. Lys 549 and Lys 708 are from the N- and C-terminal subdomains of one protomer (shown in green) respectively, and Lys 631 is from a neighboring protomer (shown in blue). ***c***, Stereo σ_A-weighted SA omit ($2F_o$ - F_c) difference map at 1.0 σ of ATP and lysines in (*a*). Both Lys 549 and Lys 708 are well-ordered and clearly defined in the experimental density map contoured at 1.1σ . Lys 631 side chain atoms are weakly present in the experimental map but are clearly visible in σ_A-weighted SA omit maps (calculated with Lys 631 side chain atoms omitted). Both figures prepared using gl-render, Bobscript and POV-ray.

NSF-D2 containing fractions, determined by SDS-PAGE, were concentrated to 2 mg ml^{-1}. 1 mg TEV protease was added per 10 mg NSF-D2, and dialyzed at 4 °C for 48 h against 500 volumes of buffer B (20 mM Tris pH 8.0, 0.1mM ATP pH 7.0, 1 mM $MgCl_2$, 10 mM β-mercaptoethanol) plus 100 mM NaCl. After dialysis and histidine tag removal, the protein was loaded onto a MonoQ column (Pharmacia) and eluted in buffer B with a linear gradient from 100–500 mM NaCl. Pure NSF-D2, as assayed by silver stained SDS-PAGE Phast gels (Pharmacia) and mass spectrometry using samples prepared in a matrix of 3,5-dimethoxy-4-hydroxycinnamic acid on a Voyager MALDI mass spectrometer (PerSeptive Biosystems), was concentrated to 4 mg ml^{-1}, dialyzed at 4 °C for 24 h against 200 volumes of buffer C (20 mM HEPES pH 7.0, 100 mM NaCl, 20 mM ADP pH 7.0, 5 mM $MgCl_2$, 2% glycerol and 20 mM dithiothreitol (DTT)), then concentrated to 15 mg ml^{-1}. Protein concentrations were determined using a Bradford protein concentration assay (Biorad) using a bovine serum albumen standard.

SeMet protein was produced essentially as above, except for the following: B834lλ(DE3) cells (Novagen) were used for expression, and were grown in SeMet-containing defined media[28] to an optical density of A_{600nm} = 1.5 before induction with 0.2 mM IPTG. Purification following Ni-NTA elution, crystallization, and cryoprotection were done under reducing conditions, with buffers, containing 20 mM DTT, extensively degassed.

Crystallization. Crystals were produced by hanging drop vapor diffusion at 4 °C. 2 ml of 15 mg ml^{-1} protein in buffer C were mixed with 2 ml of mother liquor (100 mM MES pH 6.1, 0.5 % PEG 6000) on a glass cover slip and equilibrated against 0.5 ml of mother liquor. Hexagonal, rod-shaped crystals grew to full size (approximately 200 μm × 75 μm × 75 μm) after 14 days. Crystals were cryoprotected in mother liquor supplemented with 40% PEG 400, and then flash-frozen in liquid nitrogen cooled propane. SeMet crystals were grown, cryoprotected, and frozen as above, except for a lower protein stock concentration (7 mg ml^{-1}).

Data Collection. NSF-D2 crystallizes in space group P6 with 1 protomer per asymmetric unit (Table 1). One of the native diffraction data sets and the MAD data were collected at -170 °C on beamline1-5 at the Stanford Synchotron Radiation Laboratory (SSRL) using a Quantum 4 CCD detector (Area Detector Systems Corporation) (Table 1). MAD data were collected at four wavelengths (Table 1). The second native data set was collected on beamline 19ID at the Advanced Photon Source (APS), and subsequently merged with the SSRL native data set (Table 2). All data were processed using DENZO[29] and intensities were scaled using SCALEPACK[29] (Table 1).

MAD phasing. Anomalous and dispersive diffraction ratios are shown in Table 1. Seventeen of the 18 selenium sites expected per NSF-D2 protomer were found using the Patterson heavy atom search method (R.W. Grosse-Kunstleve and A.T.B., unpublished results) as implemented in CNS[30]. MAD phasing was carried out using the Phillips-Hodgson method[31] using maximum-likelihood tar-

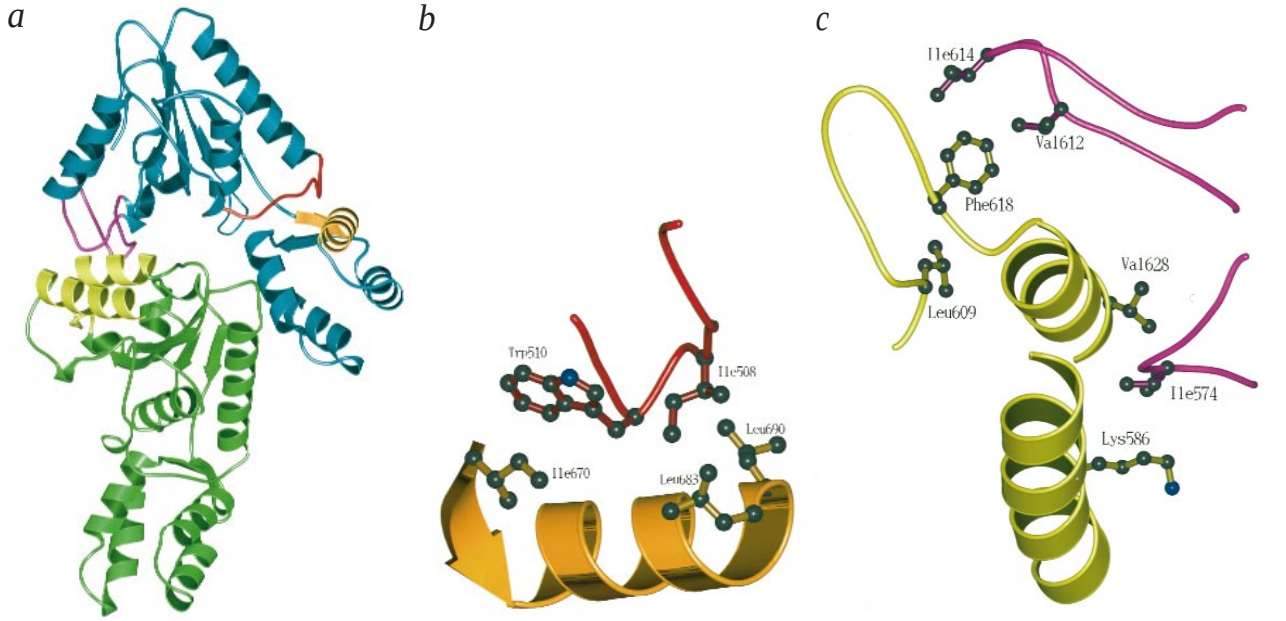

Fig. 6 ***a***, Contact regions between subdomains of a protomer, in red and orange, and between neighboring protomers, in yellow and purple. ***b***, The N-terminal and C-terminal subdomains contact through a hydrophobic patch consisting of Ile 508 and Trp 510 from the former (red), and Ile 670, Leu 682, and Leu 683 from the latter (orange). ***c***, Between N-terminal subdomains on neighboring protomers, another hydrophobic contact is formed between Ile 574, Val 612, and Ile 614 from one protomer (purple) and the β- through γ-carbons of Lys 586, Leu 609, Phe 618 and Val 628 from the other (yellow).

get functions[32] as implemented in CNS[30] (Table 1). The first N-terminal SeMet was disordered.

Model building and refinement. The initial model containing residues 23–260 was constructed from electron density maps obtained by MAD phasing and subsequent solvent-flattening[33] and histogram matching[34] along with phase extension to 1.9 Å resolution, as implemented in CNS. The high quality of the experimental map and known selenium sites allowed unambiguous tracing of the protein backbone, side chains, and ATP using the

Table 1 Crystallographic data and parameters

Crystal	Spacegroup	Cell Dimensions
Native 1	P6	a = b = 116.11 Å c = 44.24 Å
Native 2	P6	a = b = 116.09 Å c = 44.09 Å
SeMet	P6	a = b = 116.19 Å c = 44.22 Å

Crystal	d_{min} (Å)	No. of measurements	No. of unique reflections	Completeness (%)	I/σ_I	R_{sym}[1] (%)
Native 1	1.9	73,713	25,742	94.8 (83.3)	14.9	3.5 (41.8)
Native 2	1.9	107,546	46,235	96.4 (90.2)	14.2	4.0 (30.1)
SeMet λ_1 (1.0683 Å)	2.4	62,239	24,532	86.0 (63.0)	12.5	5.2 (24.4)
SeMet λ_2 (0.9800 Å)	2.4	71,022	25,463	90.0 (75.0)	10.3	5.7 (28.6)
SeMet λ_3 (0.9795 Å)	2.4	70,811	25,326	89.0 (73.0)	9.6	6.4 (31.2)
SeMet λ_4 (0.9252 Å)	2.4	72,802	25,456	89.0 (76.0)	9.9	6.2 (32.6)

Observed Diffraction Ratios[3]

	λ_1	λ_2	λ_3	λ_4
λ_1	0.084	0.093	0.089	0.081
λ_1		0.069	0.061	0.082
λ_1			0.090	0.075
λ_1				0.074

MAD phasing power[4] and figure of merit[5]

	$\lambda_1 \rightarrow \lambda_1^-$	$\lambda_1 \rightarrow \lambda_2^+$	$\lambda_1 \rightarrow \lambda_2^-$	$\lambda_1 \rightarrow \lambda_3^+$	$\lambda_1 \rightarrow \lambda_3^-$	$\lambda_1 \rightarrow \lambda_4^+$	$\lambda_1 \rightarrow \lambda_4^-$	FOM[5]
100–2.4 Å	0.19	1.43	1.52	1.16	1.33	0.42	0.61	0.56
2.5–2.4 Å	0.069	0.44	0.47	0.35	0.40	0.11	0.15	0.25

[1]Values in parentheses are for the specified high-resolution bin except where indicated.
[2]$R_{sym} = \Sigma_h \Sigma_i |I_i(h) - \langle I(h)\rangle| / \Sigma_h \langle I(h)\rangle$ where $I_i(h)$ is the i-th measurement and $\langle I(h)\rangle$ is the weighted mean of all measurements of I(h).
[3]Values for the observed anomalous diffraction ratios are $\langle\Delta|F|^2\rangle^{1/2} / \langle|F|^2\rangle^{1/2}$, where $\Delta|F|$ is the Bijvoet difference at one wavelength (diagonal elements) or the dispersive difference at the two wavelengths (intersecting at an off-diagonal element).Values are computed at 20.0–2.4 Å resolution.
[4]MAD phasing power is defined as $[\langle|F_{h1} - F_{hi}|^2\rangle / \int_\phi P_{\lambda 1 \rightarrow \lambda i}(\phi)\,(|\,|F_{\lambda 1}|e^{i\phi} + F_{hi} - F_{h1}| - |F_{li}|)^2 d\phi]^{1/2}$ for individual lack-of-closure expressions between the reflections of the reference wavelength I_1, its Friedel mate (indicated by λ_1^-) and the Friedel pairs measured at the other wavelengths (indicated by λ_i^+ and λ_i^-). F_{hi} are the heavy atom structure factors and $P_{\lambda 1 \rightarrow \lambda i}(\phi)$ is the corresponding phase probability distribution[31,48].
[5]Figure of merit.

Table 2 Refinement statistics[1]

Resolution range	50.0–1.9 Å										
No. of reflections	50,548										
Resolution (Å)	50.0–4.09	3.25	2.84	2.58	2.39	2.25	2.14	2.05	1.97	1.9	Overall
R-value[2]	21.7	20.4	22.8	22.8	23.4	22.9	22.7	24.8	25.9	28.8	22.4
R_{free}[3]	22.7	20.9	24.5	25.4	26.9	28.4	25.7	25.4	30.0	33.3	24.4
Luzzati coordinate error	0.25 Å										
Cross-validated Luzzati coordinate error	0.28 Å										
Bond-length deviation	0.007 Å										
Bond-angle deviation	1.26°										
Improper-angle deviation	0.77°										
Dihedrals	20.7°										
Average B-factor	35.5 Å^2										
Minimum B-factor	16.8 Å^2										
Maximum B-factor	75.0 Å^2										
% Residues in core phi-psi regions	91.8%										
% Residues in disallowed regions	0.0%										

[1]Using the merged native data (Native 1 + Native 2). All diffraction data were used, that is, no resolution or amplitude based cutoffs were applied.
[2]$R = \Sigma(|F_{obs}| - \kappa|F_{calc}|)/\Sigma|F_{obs}|$
[3]R_{free} is the R-value obtained for a test set of reflections, consisting of a randomly selected 10% subset of the diffraction data, not used during refinement or σ_A value calculations.

program O[35]. All refinement procedures were carried out using CNS, with progress measured using cross-validation with a 10% randomly selected test set. Initial refinement consisted of several iterations of torsion angle dynamics simulated annealing[36] using the MLHL target function with the experimental phases as a prior phase distribution[32], followed by model rebuilding in O. Later, refinement consisted of rounds of selecting chemically reasonable water molecules in phase-combined σ_A-weighted $2F_o - F_c$ maps, conjugate gradient minimization, individual restrained atomic B-factor refinement[37], and model rebuilding using experimental, σ_A-weighted, and phase combined σ_A-weighted $2F_o - F_c$[30] maps, utilizing unmodified MAD phases. Disordered side chain atoms were set to an occupancy of 0 during refinement and when computing maps. Data from 50.0–1.9 Å were used with flat bulk solvent correction[33]. Final statistics are shown in Table 2.

Coordinates. Atomic coordinates and structure factors have been deposited in the Brookhaven Protein Data Bank (accession number 1NSF).

Acknowledgments
The authors thank S.C. Stroupe and D. Fasshauer for stimulating discussions, R.B. Sutton for expert advise during the course of the project, C. Ostermeier for aid with crystallization, S.R. Sprang for critical reading of the manuscript, L. Esser for assistance in figure preparation, H. Bellamy for assistance with data collection at SSRL 1-5 (SSRL is funded by the Department of Energy, Office of Basic Energy Sciences; the SSRL Biotechnology Program is supported by the NIH, Biomedical Research Technology Program, Division of Research Resources; further SSRL support is provided by the Department of Energy, Office of Health and Environmental Research), and A. Joachimiak and the Structural Biology Center for assistance with data collection at APS (collected at the 19ID beamline of the Structural Biology Center at the Advanced Photon Source at Argonne National Laboratory: this national user facility is supported by the Office of Health and Environmental Research, U.S. Department of Energy). Support by the National Institutes of Health to A.T.B. is gratefully acknowledged.

Received 1 July, 1998; accepted 4 August, 1998.

1. Malhotra, V., Orci, L., Glick, B.S., Block, M.R. & Rothman, J.E. Role of an N-ethylmaleimide-sensitive transport component in promoting fusion of transport vesicles with cisternae of the Golgi stack. *Cell* **54**, 221–227 (1988).
2. Block, M.R., Glick, B.S., Wilcox, C.A., Wieland, F.T. & Rothman, J.E. Purification of an N-ethylmaleimide-sensitive protein catalyzing vesicular transport. *Proc. Natl. Acad. Sci. U SA* **85**, 7852–7856 (1988).
3. Haas, A. and Wickner, W. Homotypic vacuole fusion requires Sec17p (yeast α-SNAP) and Sec18p (yeast NSF). *EMBO J* **15**, 3296–3305 (1996).
4. Banerjee, A., Barry, V.A., DasGupta, B.R. & Martin, T.F.J. N-ethylmaleimide sensitive factor acts at a prefusion ATP-dependent step in Ca^{2+}-activated exocytosis. *J. Biol. Chem.* **271**, 20223–20226 (1996).
5. Mayer, A., Wickner, W. & Haas, A. Sec18p (NSF)-driven release of Sec17p (α-SNAP) can precede docking and fusion of yeast vacuoles. *Cell* **85**, 83–94 (1996).
6. Sollner, T. *et al.* SNAP receptors implicated in vesicle targeting and fusion. *Nature* **362**, 318–324 (1993).
7. Hanson, P.I., Roth, R., Morisaki, H., Jahn, R. & Heuser, J.E. Structure and conformational changes in NSF and its membrane receptor complex visualized by quick freeze/deep-etch electron microscopy. *Cell* **90**, 523–525 (1997).
8. Confalonieri, F. and Duguet, M. A 200-amino acid ATPase module in search of a basic function. *BioEssays* **17**, 639–650 (1995).
9. Beyer, A. Sequence analysis of the AAA protein family. *Prot. Sci.* **6**, 2043–2058 (1997).
10. Tagaya, M., Wilson, D.W., Brunner, M., Arango, N. & Rothman, J.E. Domain structure of an N-ethylmaleimide-sensitive fusion protein involved in vesicular transport. *J. Biol. Chem.* **268**, 2662–2666 (1993).
11. Morgan, A., Dimaline, R. & Burgoyne, R.D. The ATPase activity of N -ethylmaleimide-sensitive fusion protein (NSF) is regulated by soluble NSF attachment proteins. *J. Biol. Chem.* **269**, 29347–29350 (1994).
12. Sumida, M., Hong, R.M. & Tagaya, M. Role of two nucleotide-binding regions in an N-ethylmaleimide-sensitive factor involved in vesicle-mediated protein transport. *J. Biol. Chem.* **269**, 20636–20641 (1994).
13. Whiteheart, S.W. *et al.* N-ethylmaleimide-sensitive fusion protein: a trimeric ATPase whose hydrolysis of ATP is required for membrane fusion. *J. Cell Biol.* **126**, 945–954 (1994).
14. Nagiec, E.E., Bernstein, A. & Whiteheart, S.W. Each domain of the N-ethylmaleimide sensitive fusion protein contributes to its transport activity. *J. Biol. Chem.* **270**, 29182–29188 (1995).
15. Wilson, D.W. *et al.* A fusion protein required for vesicle-mediated transport in both mammalian cells and yeast. *Nature* **339**, 355–359 (1989).
16. Hendrickson, W.A. Determination of macromolecular structures from anomalous diffraction of synchrotron radiation. *Science* **254**, 51–58 (1991).
17. Fleming, K.G. *et al.* A revised model for the oligomeric state of the N-ethylmaleimide-sensitive fusion protein, NSF. *J. Biol. Chem.* **273**, 15675–15681 (1998).
18. Peters, J.-M., Walsh, M.J. & Franke, W.W. An abundant and ubiquitous homooligomeric ringγ-shaped ATPase particle related to the putative vesicle fusion proteins Sec18p and NSF. *EMBO J* **9**, 1757–1767 (1990).
19. Rossmann, M.G., Moras, D. & Olsen, K.W. Chemical and biological evolution of a nucleotide-binding protein. *Nature* **250**, 194–199 (1974).
20. Holm, L. and Sander, C. Protein structure comparison by alignment of distance matrices. *J. Mol. Biol.* **233**, 123–138 (1993).
21. Guenther, B., Onrust, R., Sali, A., O'Donnell, M. & Kuriyan, J. Crystal structure of the d' subunit of the clamp-loader complex of *E. coli* DNA polymerase III. *Cell* **91**, 335–345 (1997).
22. Walker, J.E., Saraste, M.J., Runswick, J.J. & Gay, N.J. Distantly related sequences in the α- and β-subunits of ATPase, myosin, kinases and other ATP-requiring enzymes and a common nucleotide binding fold. *EMBO J* **1**, 945–951 (1982).
23. Morgan, A. & Burgoyne, R.D. Is NSF a fusion protein? *Trends Cell Biol.* **5**, 335–339 (1995).
24. Boisvert, D.C., Wang, J., Otwinowski, Z., Horwich, A.L. & Sigler, PB. The 2.4 Å crystal structure of the bacterial chaperonin GroEL complexed with ATP-—S. *Nature Struct Biol* **3**, 170–177 (1996).
25. Saraste, M. and Sibbald, P.R. The P-loop-a common motif in ATP- and GTP-binding proteins. *Trends Biol Sci* **15**, 430–434 (1990).
26. Matveeva, E.A., He, P. & Whiteheart, S.W. N-ethylmaleimide sensitive fusion protein contains high and low affinity ATP-binding sites that are functionally distinct. *J. Biol. Chem.* **272**, 26413–26418 (1997).
27. Bernard, A. and Payton, M. Fermentation and growth of *Escherichia coli* for optimal protein production. In *Current Protocols in Protein Science.* (Coligan,J.E., Dunn, B.M., Plough, H.L., Speicher, D.W. & Wingfield, P.T., Eds) Chapter 5.3 (John Wiley & Sons, Inc., New York; 1995).
28. Leahy, D.J., Erickson, H.P., Aukhil, I., Joshi, P. & Hendrickson, W.A. Crystallization of a fragment of human fibronectin: introduction of methionine by site-directed mutagenesis to allow phasing via selenomethionine. *Proteins* **19**, 48–54 (1994).
29. Otwinowski, Z. In *Data Collection and Processing.* (eds Sawyer, L., Isaacs, N. & Bailey, S.) 56–62 (SERC Daresbury Laboratory, Warrington, UK; 1993).
30. Brünger, A.T. *et al.* Crystallography and NMR System (CNS): A new software system for macromolecular structure determination. *Acta Crystallogr. D*, **in the press** (1998).
31. Phillips, J.C. & Hodgson, K.O. The use of anomalous scattering effects to phase diffraction patterson from macromolecules. *Acta Crystallogr. A* **36**, 856–864 (1980).
32. Pannu, N.S. & Read, R.J. Improved structure refinement through maximum likelihood. *Acta Crystallogr. A* **52**, 659–668 (1996).
33. Jiang, J.-S. & Brünger, A.T. Protein hydration observed by x-ray diffraction: solvation properties of penicillopepsin and neuraminidase crystal structures. *J. Mol. Biol.* **243**, 100–115 (1994).
34. Zhang, K.Y.J. & Main, P. Histogram matching as a new density modification technique for phase refinement and extension of protein molecules. *Acta Crystallogr. A* **46,** 41–46 (1990).
35. Jones, T.A. Zou, J.Y., Cowan, S. & Kjeldgaard, M. Improved methods for building protein models in electron density maps and the location of errors in these models. *Acta Crystallogr. A* **47**, 110–119 (1991).
36. Rice, L.M. & Brünger, A.T. Torsion Angle Dynamics: Reduced variable conformational sampling enhances crystallographic structure refinement. *Proteins* **19**, 277–290 (1994).
37. Yu, H.-A., Karplus, M. & Hendrickson, W.A. Restrains in temperature-factor refinement for macromolecules: an evaluation by molecular dynamics. *Acta Crystallogr. D* **41**, 191–201 (1985).
38. Lenzen, C.U., Oppitz, D., Whiteheart, S.W. & Weis, W.I. Crystal structure of the hexamerization domain of N-ethylmaleimide-sensitive fusion protein. *Cell*, **in the press** (1998).
39. Kabsch, W. and Sander, C. Dictionary of protein secondary structure: pattern recognition of hydrogen-bonded and geometrical features. *Biopolymers* **22**, 2577–2637 (1983).
40. Thompson, J.D., Higgins, D.G. & Gibson, T.J. CLUSTAL W: improving the sensitivity of progressive multiple sequence alignment through sequence weighting, positions specific gap penalties and weight matrix choice. *Nucleic Acids Res.* **22**, 4673–4680 (1994).
41. Hofmann, K.& Baron, M.D. Boxshade 3.21 http://www.ch.embnet.org/software/BOXform.html (1998).
42. Esnouf, R.M. Bobscript: An extensively modified version of MolScript that includes greatly enhanced coloring capabilities. *J. Mol. Graph. Model* **15**, 132–134 (1997).
43. The POV-ray Team. Pov-ray — the persistence of vision raytracer, http://www.povray.org/ (1998).
44. Kraulis, P. MOLSCRIPT: A program to produce both detailed and schematic plots of protein structures. *J. Appl. Crystallogr.* **24**, 946–950 (1991).
45. Koradi, R., Billeter, M. & Wüthrich, K. MOLMOL: a program for display and analysis of macromolecular structures. *J. Mol. Graphics* **14**, 51–55 (1996).
46. Nicholls, A., Sharp, K.A. & Honig, B. Protein folding and association: Insights from the interfacial and thermodynamic properties of hydrocarbons. *Proteins* **11**, 281–296 (1991).
47. Jorgensen, W.L. and Rives, J.T. The OPLS potential functions for protein energy minimizations for crystals of cyclic peptide and crambin. *J. Am. Chem. Soc.* **110**, 1657–1666 (1988).
48. Burling, F.T., Weis, W.I., Flaherty, K.M. & Brünger, A.T. Direct observation of protein solvation and discrete disorder with experimental crystallographic phases. *Science* **271**, 72–77 (1996).